Water mass modification over the continental shelf north of Ronne Ice Shelf, Antarctica

K. W. Nicholls,[1] L. Padman,[2] M. Schröder,[3] R. A. Woodgate,[4] A. Jenkins,[1] and S. Østerhus[5]

Received 13 November 2002; revised 11 April 2003; accepted 5 June 2003; published 13 August 2003.

[1] We use new data from the southern Weddell Sea continental shelf to describe water mass conversion processes in a formation region for cold and dense precursors of Antarctic Bottom Water. The cruises took place in early 1995, 1998, and 1999, and the time series obtained from moored instruments were up to 30 months in length, starting in 1995. We obtained new bathymetric data that greatly improve our definition of the Ronne Depression, which is now shown to be limited to the southwestern continental shelf and so cannot act as a conduit to northward flow from Ronne Ice Front. Large-scale intrusions of Modified Warm Deep Water (MWDW) onto the continental shelf occur along much of the shelf break, although there is only one location where the MWDW extends as far south as Ronne Ice Front. High-Salinity Shelf Water (HSSW) produced during the winter months dominates the continental shelf in the west. During summer, Ice Shelf Water (ISW) exits the subice cavity on the eastern side of the Ronne Depression, flows northwest along the ice front, and reenters the cavity at the ice front's western limit. During winter the ISW is not observed in the Ronne Depression north of the ice front. The flow of HSSW into the subice cavity via the Ronne Depression is estimated to be 0.9 ± 0.3 Sv. When combined with inflows along the remainder of Ronne Ice Front (reported elsewhere), sufficient heat is transported beneath the ice shelf to power an average basal melt rate of 0.34 ± 0.1 m yr^{-1}. *INDEX TERMS:* 4207 Oceanography: General: Arctic and Antarctic oceanography; 4219 Oceanography: General: Continental shelf processes; 1827 Hydrology: Glaciology (1863); 4283 Oceanography: General: Water masses; 4536 Oceanography: Physical: Hydrography; *KEYWORDS:* Weddell Sea, High-Salinity Shelf Water, Antarctic Bottom Water, Ice Shelf Water, Ronne Ice Shelf, basal melt rate

Citation: Nicholls, K. W., L. Padman, M. Schröder, R. A. Woodgate, A. Jenkins, and S. Østerhus, Water mass modification over the continental shelf north of Ronne Ice Shelf, Antarctica, *J. Geophys. Res.*, *108*(C8), 3260, doi:10.1029/2002JC001713, 2003.

1. Introduction

[2] The long-held view that the Weddell Sea is a hot spot for the production of Antarctic Bottom Water (AABW) has been one of the principal drivers of recent research on the southern Weddell Sea continental shelf. Waters that penetrate onto the Antarctic continental shelf are modified by their interaction with both the atmosphere and the floating ice shelves. More than half of the broad southern Weddell Sea continental shelf (Figure 1) is covered by Filchner-Ronne Ice Shelf (FRIS), and it is in the ocean cavity beneath the FRIS as well as over the open continental shelf to the north that much of the conditioning of the Weddell Sea continental shelf water masses is thought to occur [*Foldvik and Gammelsrød*, 1988]. Sea ice formation salinifies water that flows onto the continental shelf, converting it into High-Salinity Shelf Water (HSSW). The sea ice drifts north in the Weddell Gyre and is removed from the shelf regime [*Harms et al.*, 2001]. The HSSW is the principal parent water mass for the production of Weddell Sea Bottom Water and Weddell Sea Deep Water, which are precursors for AABW [*Gordon*, 1998].

[3] There are three commonly cited mechanisms by which HSSW on the Weddell Sea continental shelf contributes to AABW production. First, HSSW may become dense enough as a result of brine rejection through sea ice formation to flow down the continental slope directly [*Gordon*, 1998]. Second, HSSW may mix with off-shelf water masses at the continental shelf break, enabling it to penetrate the dynamic barrier presented by the shelf break front [*Foster and Carmack*, 1976]. Finally, HSSW might first be converted to Ice Shelf Water (ISW) by interaction with the FRIS [*Foldvik and Gammelsrød*, 1988] and possibly also with the Larsen Ice Shelf on the western Weddell

[1]British Antarctic Survey, Natural Environment Research Council, Cambridge, UK.
[2]Earth and Space Research, Seattle, Washington, USA.
[3]Alfred Wegener Institute for Polar and Marine Research, Bremerhaven, Germany.
[4]Applied Physics Laboratory, University of Washington, Seattle, Washington, USA.
[5]Geophysical Institute and Bjerknes Centre for Climatic Research, University of Bergen, Bergen, Norway.

0148-0227/03/2002JC001713$09.00

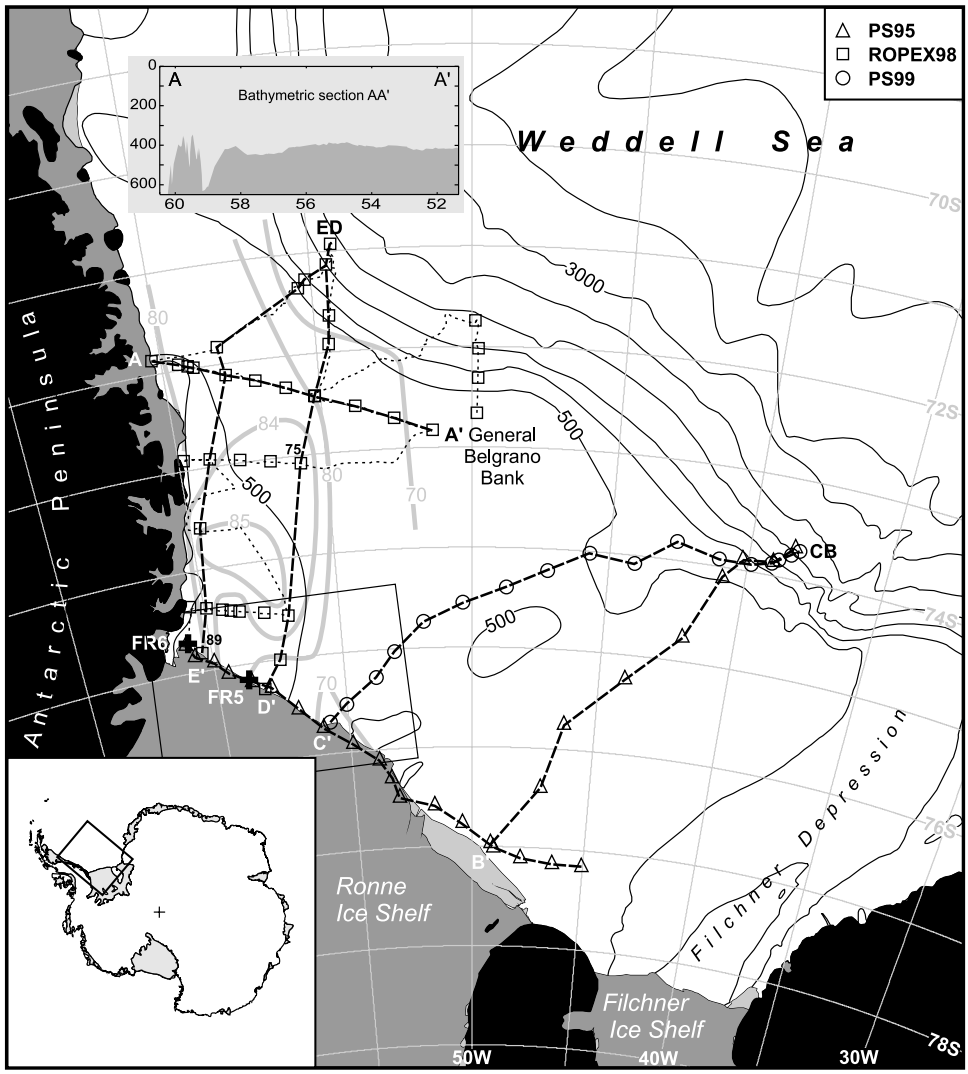

Figure 1. Map showing the southern Weddell Sea study area, including the seaward portions of Ronne and Filchner Ice Shelves. The black contour lines show bathymetry in meters [*British Antarctic Survey*, 2000]. Triangles, squares, and circles show the locations of CTD profiles obtained during PS95, ROPEX98, and PS99, respectively, which are used in the paper. Dashed lines connecting letters (AA′, for example) show the main CTD sections discussed in the text. The dotted line is the ship track over the Ronne Depression for the ROPEX98 cruise, data from which were used during the construction of the new bathymetry for the area. The shaded lines over the Ronne Depression are contours of salinity at the seabed, expressed as $(S - 34) \times 100$, from the ROPEX98 CTD stations. The inset diagram illustrates the bathymetry with a section along the CTD transect AA′. Crosses indicate the locations of moorings FR5 and FR6 near the northwestern end of Ronne Ice Front. A box over western Ronne Ice Front indicates the area covered by the larger-scale map in Figure 2.

Sea continental shelf [*Muench and Gordon*, 1995]. ISW is less saline than HSSW as a result of the addition of fresh water from melting at the ice shelf base, but it is colder: It has, by definition, a temperature lower than the surface freezing point. It is believed that the descent of ISW down the continental slope north of Filchner Ice Shelf is aided by the thermobaric effect [*Foldvik et al.*, 1985b]. HSSW converted to ISW by interaction with the ice shelf ultimately forms a version of Weddell Sea Deep Water that is less saline than if the ice shelf plays no role [*Gordon et al.*, 1993].

[4] Evidence for the descent of unmodified HSSW has been obtained near the western Weddell continental shelf adjacent to Larsen Ice Shelf [*Gordon*, 1998]. Production of bottom waters by the shelf break mixing process has been observed in various locations around the continent [*Baines and Condie*, 1998], including the southern Weddell Sea [*Foster and Carmack*, 1976]. We focus in this paper on the processes that underpin the third mechanism, involving the ice shelf. A plume of ISW that emerges from beneath Filchner Ice Shelf, traverses the continental shelf, and then descends the continental slope near 35°W has

Table 1. Details of Instrument Records From Moorings FR5 and FR6[a]

Instrument ((Type) Serial Number)	Depth, m	Start Date	Length, days	Sensors	Mean u, cm s^{-1}	Mean v, cm s^{-1}
			FR5 (75°9.8′S, 58°43.6′W)			
(AI) 10003	204	15 Feb. 1995	816	*u*, *v*, *T*, *P*	−2.77	−0.07
(AI) 9995	305	15 Feb. 1995	830	*u*, *v*, *T*, *P*	−1.91	0.65
(NB) 1282	551	29 June 1995	545	*u*, *v*, *T*	1.54	0.34
			FR6 (74°42.3′S, 60°48.6′W)			
(AI) 0927	261	16 Feb. 1995	816	*u*, *v*, *T*, *P*, *C*	−3.72	−4.65
(AI) 9187	442	16 Feb. 1995	830	*u*, *v*, *T*	−3.42	−4.09
(NB) 1288	588	16 Feb. 1995	679	*u*, *v*, *T*	−3.30	−3.10

[a]The instrument types were Aanderaa Instruments RCM7 (AI) and Neil Brown ACM (NB). As in the text, u is the current component resolved along the ice front (toward Berkner Bank) and v is the component normal to the ice front (toward the open Weddell Sea).

been well documented from a number of cruises. Well-defined cores of ISW have also been observed farther to the west, at the western Ronne Ice Front [e.g., *Gammelsrød et al.*, 1994], but the fate of these cores has never before been determined. We have no knowledge of how the HSSW distribution and properties change with the seasons. Indeed, difficult sea ice conditions have hitherto denied us knowledge even of the summertime distribution of HSSW over the western portion of the southern continental shelf. This dearth of data is particularly important as it is at the western end of Ronne Ice Front that HSSW is observed to be most dense and therefore most effective at driving a circulation beneath the ice shelf.

[5] During the 1997–1998 austral summer the southern Weddell Sea continental shelf experienced extraordinarily light sea ice conditions [*Ackley et al.*, 2001]. The southern ice edge retreated north to near the continental shelf break, a retreat unprecedented during the satellite era and one that has not recurred in subsequent summers. During this period the Royal Navy's ice patrol vessel HMS *Endurance* carried out the 1998 Ronne Polynya Experiment (ROPEX98) in the southern Weddell Sea. One element of ROPEX98 consisted of conductivity-temperature-depth (CTD) profiling of the water column over the western part of the shelf and along Ronne Ice Front. This is the first time a research cruise has visited the western portion of the southern continental shelf to collect bathymetric and oceanographic data [*Nicholls et al.*, 1998].

[6] Instrument moorings that had been deployed at the ice front during the 1995 cruise of *Polarstern* were recovered during ROPEX98. The two moorings on which we report in this paper are the first long-term oceanographic records to be obtained from the western Ronne Ice Front [*Woodgate et al.*, 1998]. Two additional hydrographic data sets are also discussed. CTD profiles were obtained from the ice front region during *Polarstern*'s 1995 cruise (AntXII/3, hereinafter referred to as PS95) and also during her cruise in the 1998–1999 field season (AntXVI/2, hereinafter referred to as PS99). PS95 data from CTD stations occupied to the east of our study area have been presented by *Grosfeld et al.* [2001]. The three ice front CTD data sets bracket the time series obtained from the instrument moorings (up to 2.5 years in length) and highlight similarities and differences in summer conditions from one year to the next.

[7] The aims of this paper are to (1) present bathymetric and hydrographic findings from the region north of the western Ronne Ice Front; (2) determine which of the summer-observed ice front features are transient and which are present year round; (3) estimate fluxes of HSSW beneath the ice shelf from the Ronne Depression; and (4) determine the fate of ISW leaving the ice front in the Ronne Depression.

[8] In section 2 the data are used to make broad observations about the regional hydrography and the mean and seasonal circulation observed at the instrument moorings. A more detailed study of the conditions at the ice front is given in section 3, including a discussion of the fate of ISW in the Ronne Depression. Section 4 contains estimates of the total heat flux beneath Ronne Ice Front and the average ice shelf basal melt rate that this can power.

2. General Observations

[9] The data sets from the moored instruments are summarized in Table 1. All instruments measured currents and temperature. The shallowest instrument on the western mooring (FR6) was also equipped with a conductivity cell. Locations for the CTD profiles discussed in this paper are shown in Figures 1 and 2. Figure 2 shows an enlargement of the ice front region and indicates the locations of CTD stations occupied in the immediate vicinity of the ice shelf as well as the locations of moorings FR5 and FR6. The CTD profiles from ROPEX98 were obtained using a Seabird SBE-911 Plus CTD system, together with a General Oceanics 12-bottle rosette and an SBE-35 Deep Sea High Precision Thermometer. Profiles from the *Polarstern* cruises were measured using a Falmouth Scientific Instruments Triton ICTD with a General Oceanics 24-bottle rosette. The water samples were analyzed for salinity to calibrate the conductivity sensors, and samples from the ROPEX98 cruise were also analyzed for $\delta^{18}O$. Salinities were determined using a Guildline Autosal salinometer, and all values were calculated using the Practical Salinity Scale [*Lewis*, 1980]. Salinities and temperatures (in °C) have an estimated accuracy of better than 0.003.

[10] The orientation of the ice front shown in Figures 1 and 2 is thought to be accurate, although its location varies throughout the period covered by the data sets, moving approximately northeast at a speed of ~1 km yr^{-1}. A

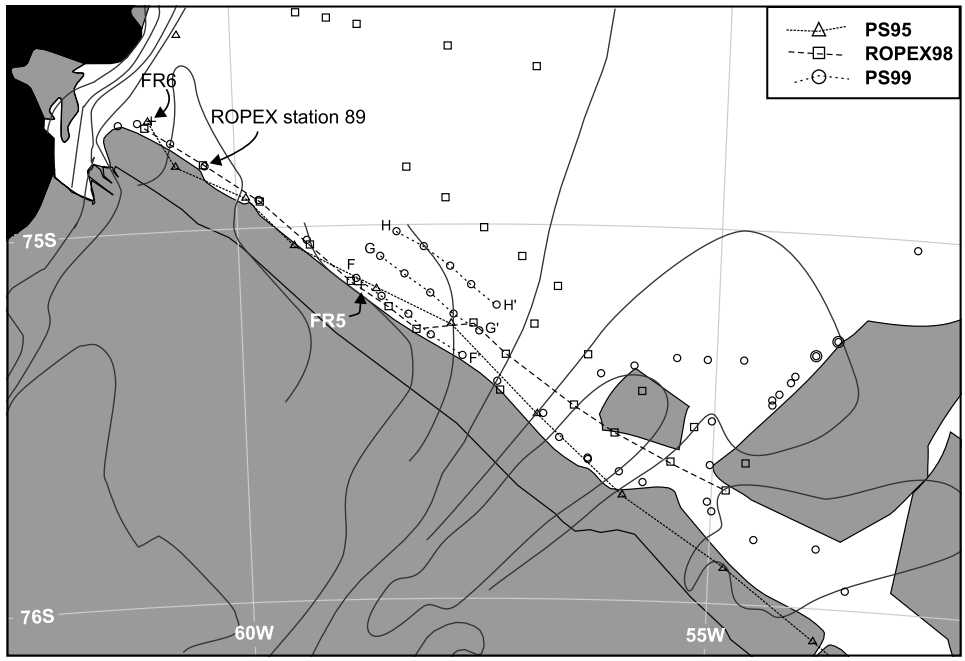

Figure 2. Large-scale map of the ice front region of northern Ronne Ice Shelf, showing the locations of CTD stations in the near vicinity of the ice front, which are used in this paper. The positions occupied by the icebergs that calved in late 1998 are shown for the period of the PS99 cruise. As in Figure 1, triangles, squares, and circles show stations occupied during PS95, ROPEX98, and PS99, respectively. The contours of bathymetry near the ice front are from the work of *Vaughan et al.* [1994]. Dashed lines indicate the CTD sections discussed in the text. The locations of the ice front are from the work of *Vaughan et al.* [1994] to represent the approximate configuration during the PS95 and ROPEX98 cruises and from the *British Antarctic Survey* [2000] for the PS99 cruise.

major iceberg calving event occurred between ROPEX98 and PS99 when the eastern third of Ronne Ice Front broke out. Both the old (pre-PS95 and ROPEX98) and new (PS99) ice fronts are shown in Figures 1 and 2, and the major icebergs present during PS99 are indicated in Figure 2.

2.1. Bathymetry

[11] The shaded, dotted line in Figure 1 shows part of the track of the *Endurance* during ROPEX98. The portion shown is over the area of the Ronne Depression that had not previously been charted. Bathymetric data from the ROPEX98 cruise have been incorporated into a new map of the Antarctic Peninsula and Weddell Sea [*British Antarctic Survey*, 2000]. The contours from that map have been included in Figure 1, highlighting the principal bathymetric finding from the study: the absence of an extension of the Ronne Depression (Figure 1) from the ice front all the way to the continental shelf break. In this way, the topography differs from the Filchner Depression, which intersects the continental shelf break north of Filchner Ice Shelf to form a well-defined sill.

[12] The new bathymetry data indicate that General Belgrano Bank, hitherto thought to be a significant bathymetric feature at the northeastern extreme of the Ronne Depression (73°S, 50°W), is only a small (~20 m) rise in the generally flat outer shelf. This significant change in shelf edge geometry has potentially significant implications for the along-slope mean flows and also for the strength of tidal currents along the shelf break that may provide much of the energy for water mass mixing at the Antarctic Slope Front [*Padman et al.*, 1998].

2.2. Hydrography

[13] The location of the PS95 ice front CTD section, which extended along most of Ronne Ice Front, is indicated by one of the dashed lines in Figures 1 and 2. Triangles represent individual stations. The θ and S distributions for the section are shown in Figure 3a. The CTD sections plotted in Figures 3b and 3c follow the line of squares (ROPEX98) and circles (PS99) along the ice front in Figure 2. In the ice front sections a perennial feature is the ISW located at the eastern margin of the Ronne Depression (Figures 3a–3c) [see *Foldvik et al.*, 1985a; *Gammelsrød et al.*, 1994]. The ISW is a water mass that has been cooled below the surface freezing point by contact with ice at depth: The freezing point of seawater decreases by ~0.75°C for every km increase in depth [*Millero*, 1978]. Farther to the west the conditions at the ice front are dominated by HSSW, with the highest observed near-bottom salinities of 34.84 during PS95 and the ROPEX98 cruise and 34.87 during PS99. Figure 4 shows the θ, S, and surface freezing point (T_{f0}) profiles from ROPEX98 station 89, toward the western side of the Ronne Depression (Figure 2). The highest salinity is near the seafloor, and ISW is found in a core near 280 dbar. The deepest 200 m of the water column is HSSW. Historically, all sections from along the ice front (including those presented here) have been obtained during late summer, the

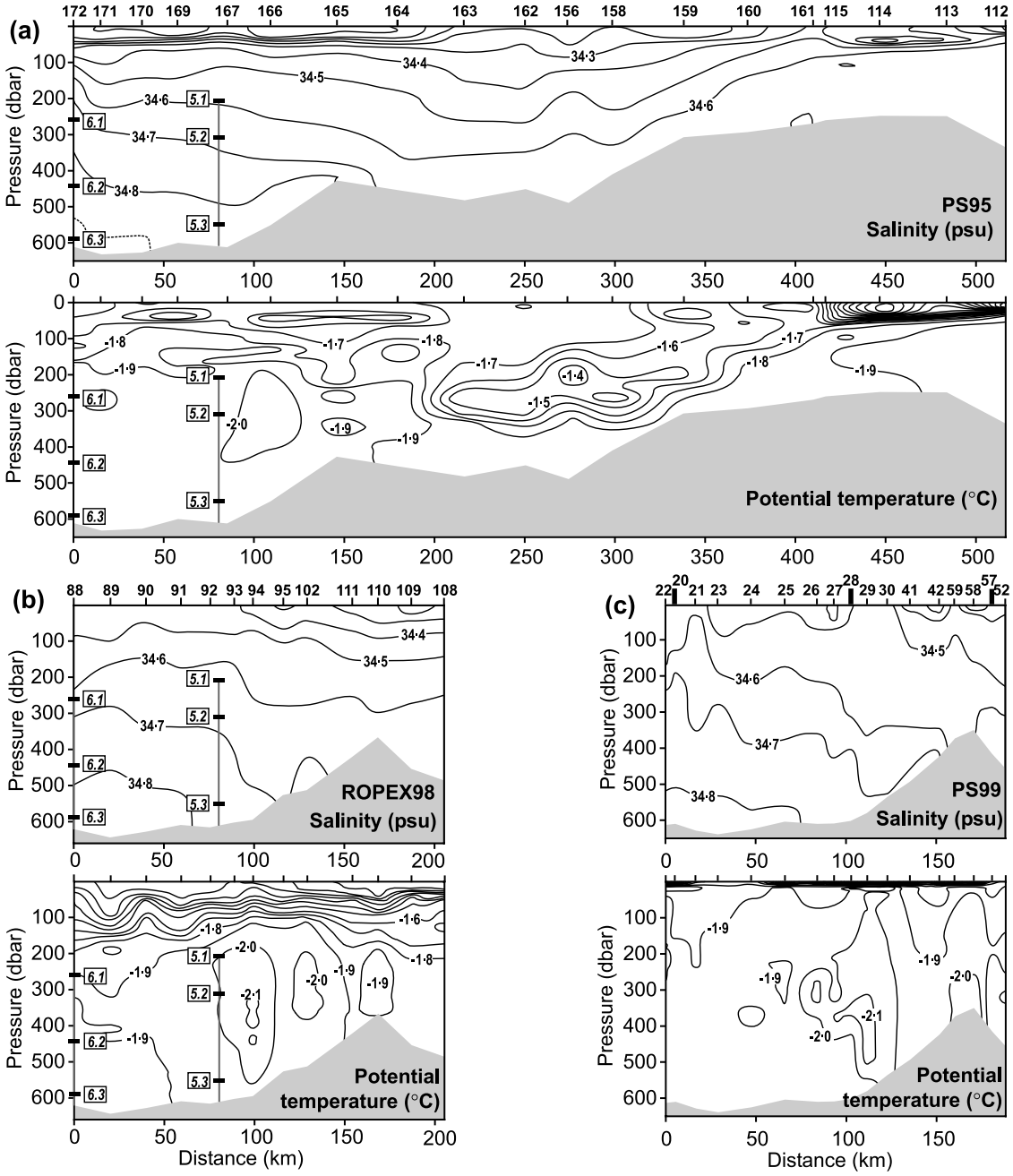

Figure 3. Contour plots of θ and *S* for sections along the ice front occupied during (a) PS95, (b) ROPEX98, and (c) PS99. The distance is measured from approximately the same point near the coast of the Antarctic Peninsula. The locations of instruments on the FR5 and FR6 moorings are shown in Figures 3a and 3b. The depth of each instrument is given in Table 1.

only part of the season when sea ice conditions generally permit access to the shore lead that is usually present at the ice front.

[14] Dashed lines in Figure 1 indicate the CTD sections plotted in Figures 5 and 6. To help define the various water masses that we discuss, Figure 7 shows a plot of θ versus *S* for all the stations occupied on the western Weddell continental shelf (Figures 1 and 2) during ROPEX98, with our definitions of different water masses identified. The section along AA′ (Figures 5a and 6a) shows Modified Weddell Deep Water (MWDW) at the eastern side of the area under study. The MWDW results from Weddell Deep Water penetrating onto the continental shelf after mixing with Winter Water, the remnant of winter convection. In Figures 5a and 6a the MWDW starts at ∼150 m depth at 55°W (∼160 km on AA′) and then expands as a layer that deepens and thickens away from the coast. The western end of the intrusion of MWDW is clearly visible in section DD′ (Figures 5d and 6d) as an elongated tongue of warmer water penetrating across the shelf and shoaling to the south as far as station 75 (Figure 1). The tongue of

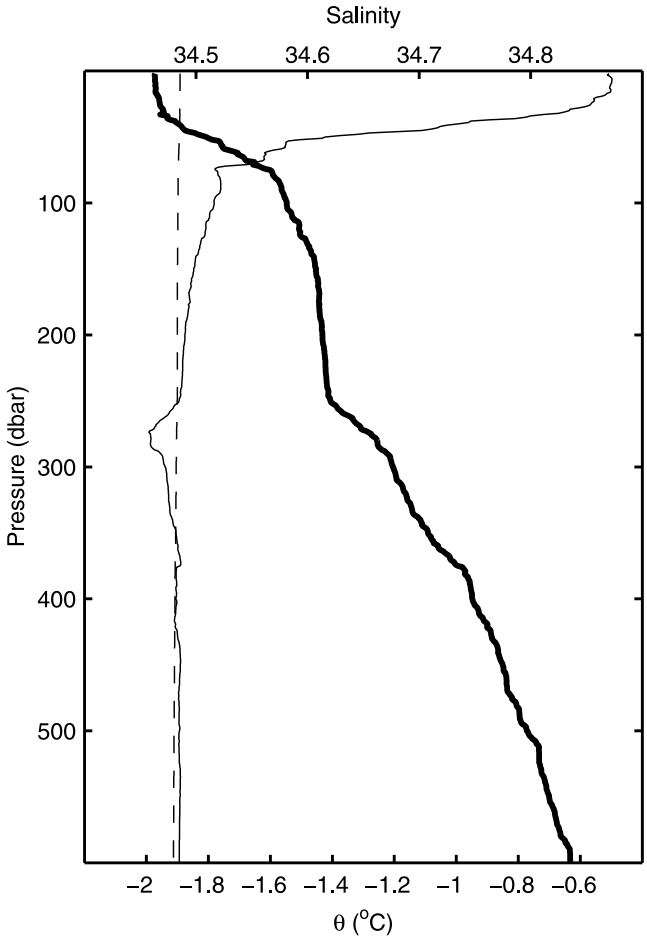

Figure 4. Vertical profiles of θ (thin line) and *S* (bold line) for ROPEX98 station 89. Also shown is the profile of the freezing point at the surface pressure (dashed line).

MWDW loses its θ-*S* identity as it reaches the surface layers, presumably as a result of interaction with sea ice and the atmosphere. PS95 and PS99 provided two further lines of CTD stations across the continental shelf farther to the east (Figure 1). Sections from these stations are shown in Figures 5b and 6b and in Figures 5c and 6c, respectively. The section from PS95 (BB′, farthest east) follows the core of MWDW that reaches the ice front, which is clearly visible in the full PS95 section along the ice front (Figure 3a). MWDW at this ice front location (∼53°W, or at 270 km in Figure 3a) has been seen every time ships have made observations in the shore lead, and this eastern core presumably occurs annually. The section from PS99 (CC′, Figures 5c and 6c) shows MWDW extending onto the shelf about as far as seen during the ROPEX98 cruise. The sections shown in Figures 5b–5d and 6b–6d were obtained during different summers and so cannot simply be combined to provide a picture of the summer distribution of MWDW. They strongly suggest, however, that east of 55°W (∼160 km on AA′), MWDW has widespread access onto the shelf, at least during summers.

[15] In the far west of the study area the front separating HSSW from off-shelf waters is clearly visible at the continental shelf break (Figures 5e and 6e), although the station separation is too large to determine the front's precise position. One of the key findings from the ROPEX98 cruise is that the far western continental shelf (Figures 5e and 6e) is dominated by HSSW even at this late stage in the summer (the stations were occupied in late January). All of the ROPEX98 stations (squares in Figures 1 and 2) were used to construct the contours of salinity at the seabed, shown in Figure 1. In general, the highest salinities were found in the deeper parts of the depression, although the maximum in bottom salinity is located north of the ice front. Figures 5d–5e and 6d–6e show that the HSSW appears to be blocked from entering the subice shelf cavity where the ISW is observed (in the vicinity of point D′, Figure 1), but there appears to be free access at the western end of the ice shelf.

2.3. Records From Moored Instruments

[16] Figures 3a and 3b show the positions of the moored instruments in the θ and *S* sections measured in the austral summers of 1995 and 1998, the two seasons that bracket the deployment period. Mooring FR5 was located at the western edge of the ISW core observed on the eastern flank of the Ronne Depression. The records from the temperature sensors at positions FR5(204 m) and FR5(305 m) (Figure 8) show that the ISW core is not a permanent feature but appears at the mooring location only during the summer, which is when sea ice conditions allow ships to visit the shore lead. For most of the year the temperature remains at the surface freezing point (approximately −1.9°C). The temperature recorded by the deepest instrument on mooring FR5, FR5(551 m), shows little variability, though it bears some similarities to the FR5(305 m) record.

[17] The temperature record from the shallowest instrument on the western mooring (FR6(261 m), Figure 8) shows features similar to those from FR5(204 m), except that the ISW appears later in the summer, generally after ships have left the area. Unlike at FR5, at FR6 the ISW signal was heavily suppressed during the 1996–1997 summer. Deeper in the water column the record from FR6(442 m) shows only a very weak ISW signature at any time. The ISW features in the temperature records from both FR5(305 m) and FR6(442 m) generally lag the equivalent event in the records from FR5(204 m) and FR6(261 m) by ∼30–40 days, respectively. The temperature recorded by the deepest instrument on FR6 (FR6(588 m)) shows the water remaining at the surface freezing point throughout the time series.

[18] Progressive vector diagrams from each instrument have been plotted in Figure 9, in which the line of the ice front has been oriented horizontally. The time series used to generate the diagrams were of different lengths and so the different speeds of flow are not represented. The diagrams show a strong component of flow along the ice front, east to west, at most of the instruments. An exception is the deepest instrument on FR5, which indicates a flow in the opposite direction. Inspection of the bathymetric contours included in Figure 2 suggests that the water at the seafloor at FR5 is flowing along contours of constant depth, which are locally parallel to the ice front. Those contours would serve to guide the water around to

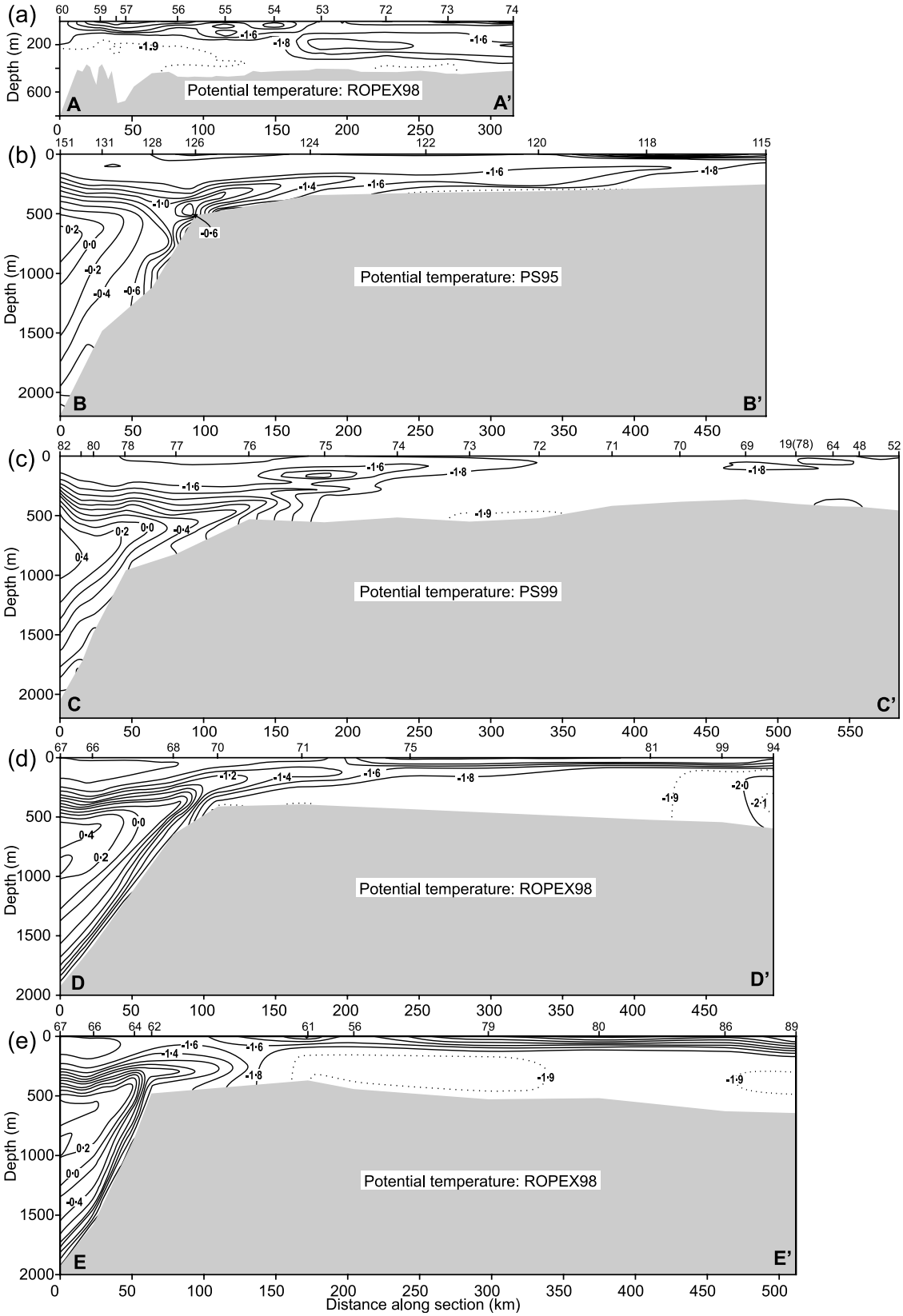

Figure 5. Contour plots of potential temperature θ for the CTD sections (a) AA′, (b) BB′, (c) CC′, (d) DD′, and (e) EE′ (Figure 1). For θ greater than −1.8°C, contour intervals are 0.2°C. Below −1.8°C they are every 0.1°C, and the contours are dotted lines.

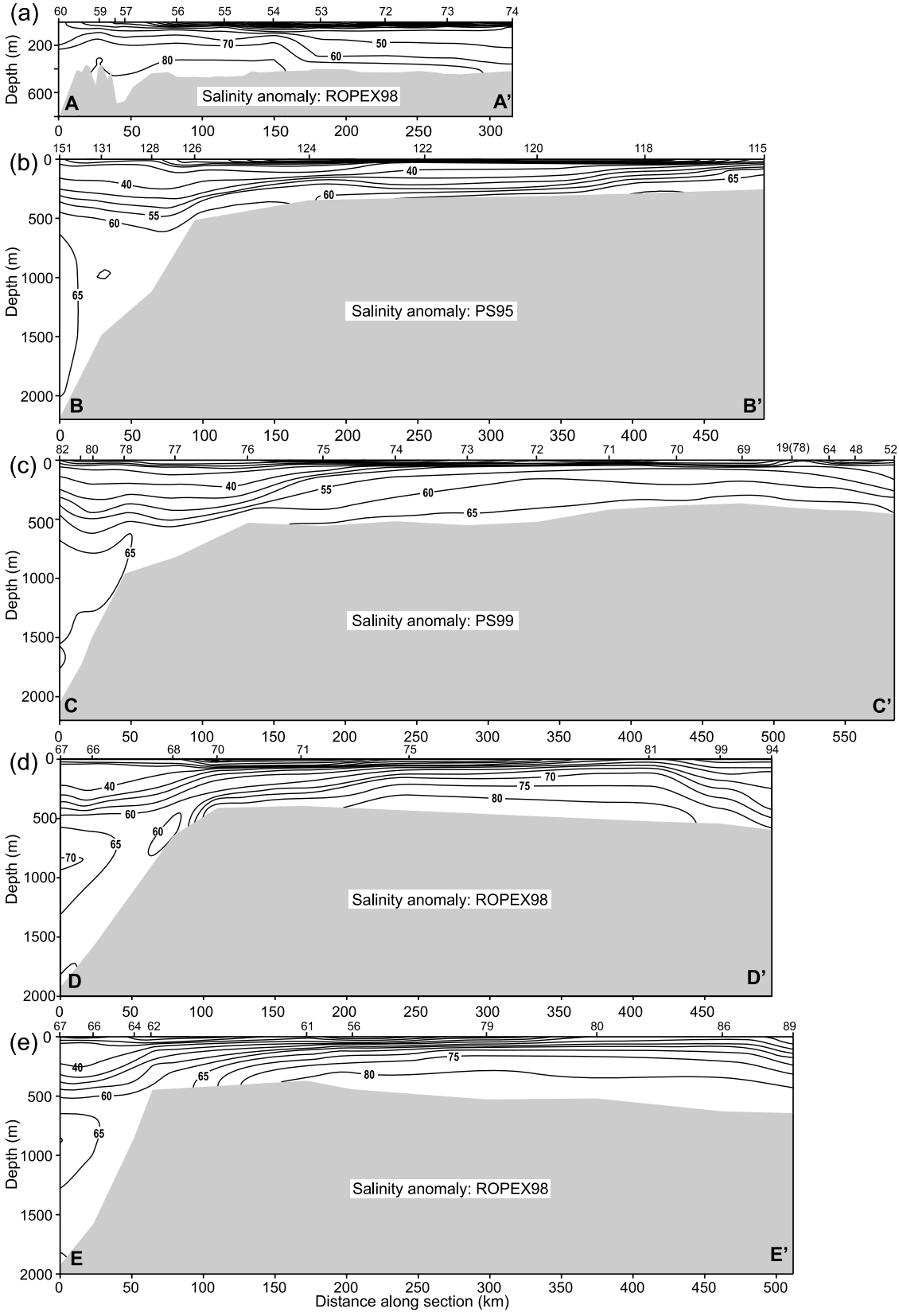

Figure 6. Same as Figure 5, but for salinity anomaly S. Contours of S are every 0.05, except for AA′, where they are every 0.1. Salinity contour values are expressed as $(S - 34) \times 100$.

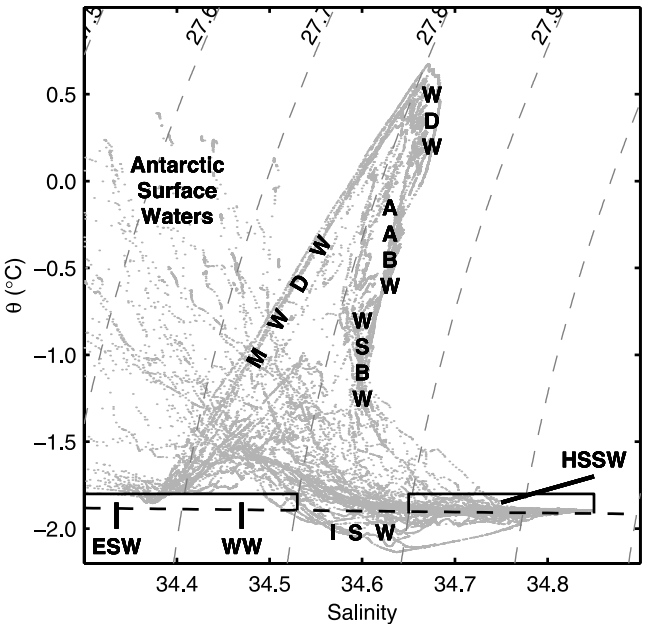

Figure 7. θ-*S* plot of the CTD profiles obtained from the southwestern Weddell Sea continental shelf during the ROPEX98 cruise. Approximate characteristics of water types referenced in the text are indicated: WSBW, Weddell Sea Bottom Water; WDW, Weddell Deep Water; AABW, Antarctic Bottom Water; HSSW, High-Salinity Shelf Water; ESW, Eastern Shelf Water; MWDW, Modified Weddell Deep Water; and WW, Winter Water.

the southeast, beneath the ice shelf and up against the eastern flank of the Ronne Depression. At FR5(204 m) the flow is directed along the ice front, with a small component out from beneath the ice shelf at FR5(305 m). At the western end of the ice front, instruments on FR6 show a net flow that always has a strong component directed beneath the ice shelf throughout the water column.

[19] Bottom salinity at Ronne Ice Front generally increases along the front from east to west [e.g., *Foldvik et al.*, 1985a], but the highest bottom salinities in the Ronne Depression are found some distance north of the ice front, near the Antarctic Peninsula coast (Figure 1). The progressive vector diagrams offer an explanation for this structure. Lower-salinity HSSW from the Berkner Bank is advected roughly along the front northwestward toward the Antarctic Peninsula, blocking the direct passage of most high-salinity HSSW into the sub-ice shelf cavity. This interpretation implies that the current along the ice front remains close to the ice shelf, without a significant off-shelf flux onto the open continental shelf. That is, ISW coming out from the ice shelf cavity on the eastern side of the Ronne Depression simply circulates counterclockwise to reenter the cavity near the western limit of the ice front.

[20] The time series from the six current meters (FR5(204 m), FR5(305 m), FR5(551 m), FR6(261 m), FR6(442 m), FR6(588 m)) are shown in Figure 10. The data have been low-pass filtered, with a cutoff at 30 days to highlight any seasonal and interannual signals. The coordinates have been rotated clockwise by 40° in order to resolve the velocities along *u* and normal *v* to the ice front. Thus a positive *u* component indicates a flow along the ice front from the Antarctic Peninsula toward Berkner Island. There is a strong tidal signal superimposed on the records (not discussed here [see *Woodgate et al.*, 1998]). The proximity of the step change in water column thickness resulting from the ice front might suggest a significant contribution to the total flow from tidal residual currents. However, *Makinson and Nicholls* [1999] show that tidal residuals are very small west of ~58°W.

3. Ice Front Conditions

3.1. Summer Hydrography From Cruises

[21] Figure 11 shows θ-*S* plots for the stations in the vicinity of the ice front that were occupied during the three cruises. Also shown is the surface freezing line $T_f(S)$, which is nearly horizontal on these plots. HSSW is formed as a direct result of sea ice production and so we expect the most saline waters to lie along this line. During the PS95 and PS99 cruises, for example, θ for the most saline HSSW lies between 0.001°C and 0.003°C of the surface freezing point, respectively. For the ROPEX98 cruise, however, θ for the most saline water lies ~0.018°C above the surface freezing point (Figure 11b). Post-ROPEX98 cruise calibration of the SBE35 precision thermometer showed insignificant instrumental drift during the cruise, and the calibrated temperature sensor on the SBE911 Plus CTD instrument agreed at submillidegree level with the SBE35. We therefore believe the offset to be a real phenomenon.

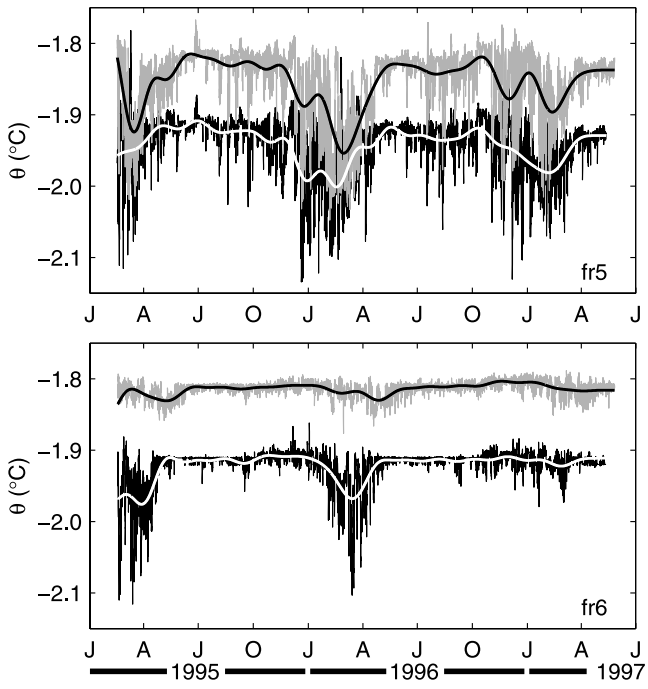

Figure 8. Potential temperature time series from instruments (top) FR5(204 m) (black) and FR5(305 m) (shaded) and from (bottom) FR6(261 m) (black) and FR6(442 m) (shaded). Both the time series and low-pass-filtered versions of the signals have been plotted. The data from FR5(305 m) and FR6(442 m) have been offset by 0.1°C to improve clarity.

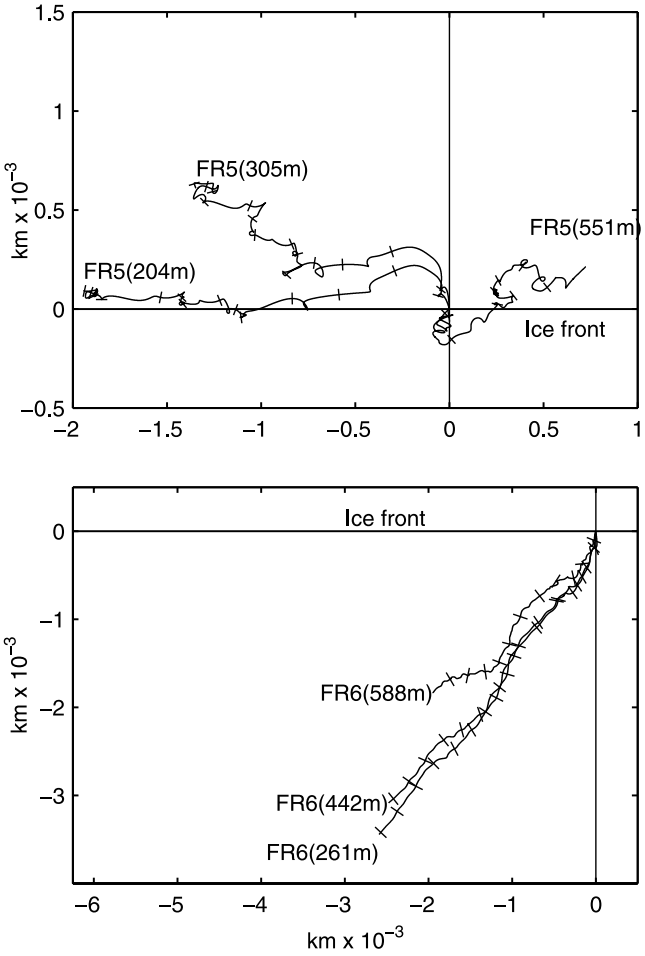

Figure 9. Progressive vector diagrams from the current meters deployed at FR5 and FR6. The 2-monthly tick marks are included on each trace.

[22] The origin of the offset presumably has its roots in the unusual conditions that led to the extraordinary open water extent during the year of the ROPEX98 cruise. In late 1997 the Weddell Sea spring was marked by an unusually sustained period of southerly winds which cleared much of the sea ice from the southern continental shelf [*Hunke and Ackley*, 2001]. Loss of ice through advection rather than melt means that the water column remained unstratified. The large available fetch would then have allowed wind stirring to be effective at mixing insolation down through the upper few tens of meters of the water column. For seawater near its freezing point, temperature acts largely as a passive tracer, having insignificant impact on the density stratification. Mixing of the heat throughout the entire water column might then be accomplished by tidal stirring. If the early summer solar gain occurred over a period of $\sim$1 month, for example, the heat necessary to warm a 500-m-thick water column by 0.018°C could be delivered by a modest average input of $\sim$15 W m^{-2}. *Renfrew et al.* [2002] show that in this region the net radiant heating in open water is more than 10 times this from as early as mid-November. As the summer progressed, precipitation and melting of any remaining sea ice would eventually create a surface layer that would inhibit further overturning.

[23] Also shown on the plots in Figure 11 is a line whose slope shows the trajectory taken by the θ-S properties of a water parcel as it interacts with the base of the ice shelf [e.g., *Gade*, 1979]. Assuming that the source water for ISW observed beneath the ice shelf is HSSW, which was therefore at or near the surface freezing point, the salinity of the ISW's parent HSSW is given by the intersection between the surface freezing line and a "Gade line" that passes through the ISW's θ-S characteristic. The additional assumptions here are that the ISW detected at the ice front has not been first modified by direct or indirect contact with the atmosphere and that its source is not a blend of HSSW masses of different or varying salinity (in which case the

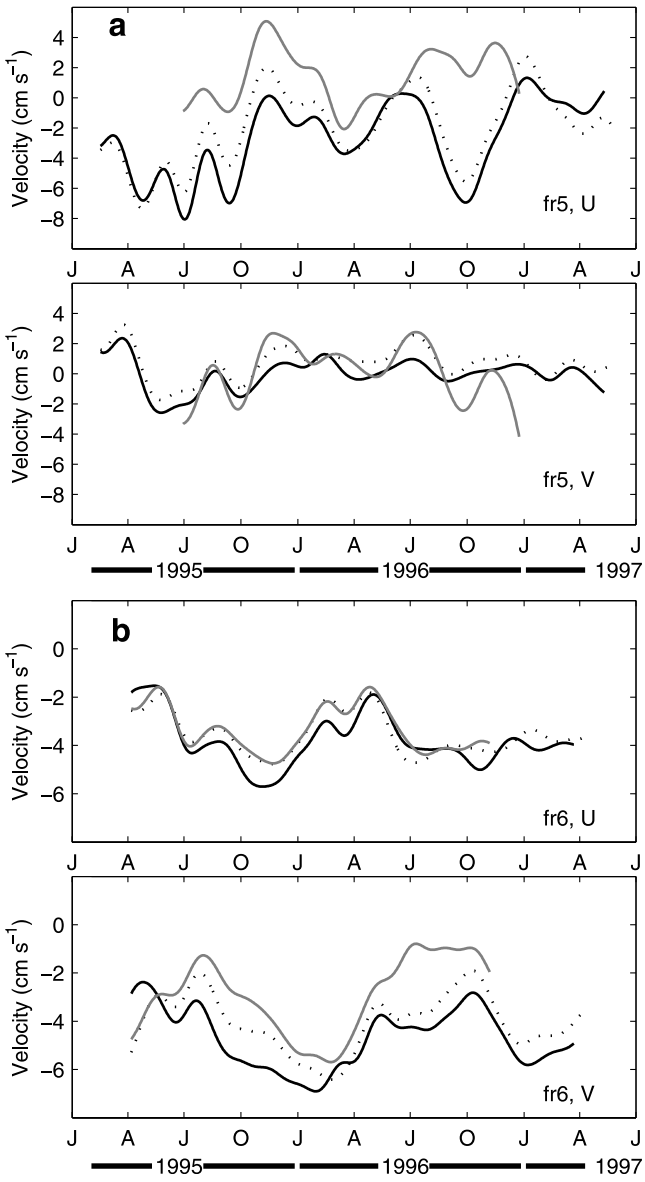

Figure 10. Low-frequency components of the (top) along-ice front (u, approximately southwest) and (bottom) cross-ice front (v, approximately northeast) velocity components for (a) instruments on mooring FR5 and (b) instruments on mooring FR6. The solid, dotted, and shaded lines are the time series from the shallowest, mid-depth, and deepest instruments, respectively.

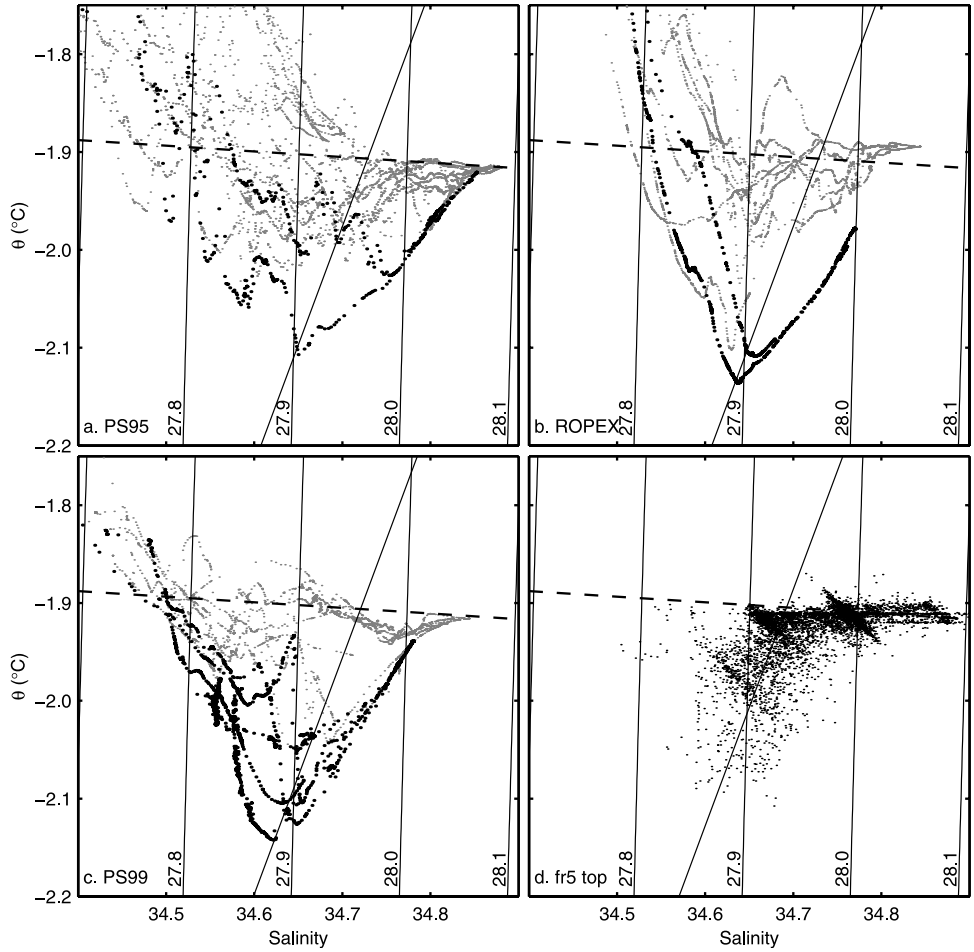

Figure 11. θ-*S* diagrams for the data from near-ice front profiles from (a) PS95, (b) ROPEX98, and (c) PS99. Data indicated by a darker point are from profiles in the vicinity of the well-defined, cold ISW plume emerging at the eastern side of the Ronne Depression. (d) θ-*S* diagram for the data from the upper instrument on mooring fr6. The dashed line in each diagram shows the surface freezing point, and the solid line is the appropriate Gade line, with an offset chosen so that the line passes through the coldest ISW.

intersection would yield the mean salinity). In addition, if, as found during ROPEX98, the HSSW temperature deviates from the surface freezing point, then there will be a small correction to be made.

[24] The θ-*S* diagrams for all three cruises suggest that the densest, most saline HSSW is not the parent water mass for any of the ISW found north of the ice front during the summer. The θ-*S* characteristics of ISW have been measured at various locations beneath the ice shelf using hot water-drilled access holes [*Nicholls et al.*, 2001; *Nicholls and Makinson*, 1998]. By drawing the appropriate Gade line, they found that the salinity of HSSW implicated as the source water for the subice shelf ISW was always less than ~34.78. Again, this strongly suggests that the highest-salinity HSSW over the Ronne Depression ($S > 34.78$) either fails to gain access to the subice shelf cavity or, if it does gain access, it never interacts directly with the ice shelf base.

[25] The coldest ISW was found in the well-defined plume emerging on the eastern side of the Ronne Depression (Figure 3). In Figures 11a–11c the θ-*S* data from stations in and near this plume are highlighted. Using a Gade line, we see that the salinity of the source water for this plume lies between 34.72 and 34.74. The warmer ISW deeper in the water column, which appears to have higher source salinity, is most likely a result of mixing between the main plume and HSSW near the bottom.

[26] Farther to the west, ISW appears in the water column at various depths, with a more distinct signal usually visible at the depth of the ice shelf base. The characteristics of the more westerly ISW signals suggest a parent water mass with a lower salinity, consistent with local water from around the depth of the ice shelf base being advected southward beneath the ice front, possibly as a result of tidal activity.

3.2. High-Salinity Shelf Water (HSSW) Production and Pathways for Ice Shelf Water (ISW)

[27] During the freezing seasons, when production of HSSW is at its most intense, all velocity records from both moorings show enhanced energy at periods between 1 and 4 days. Figure 12 shows this feature in the along-ice front

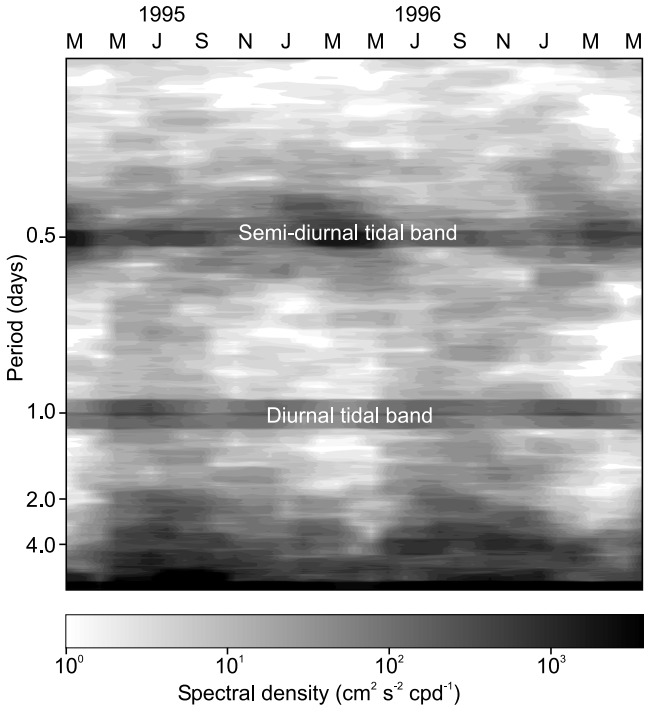

Figure 12. The spectral power density in the along-ice front current component in the record from instrument FR6(442 m). Spectra were estimated for 85.3-day intervals, each interval overlapping the last by 42.7 days. Note the enhanced energy during the winter months, particularly at periods of between 1 and 4 days.

component from instrument 6.2, for example. We ascribe this enhanced activity to baroclinic eddies generated by instabilities in a front at the edge of the region of HSSW production. Such an interpretation is consistent with the results of recent studies of dense water production in coastal polynyas [e.g., *Chapman*, 1999]. We discount shelf edge waves as being responsible for the variability: The strength of the along-shelf component of velocity is not in phase with the strength of the variability (compare Figures 10 and 12).

[28] Figure 13 shows the direction and strength of the flow at the shallowest and deepest current meters at FR6. For these plots the data have been filtered using a low-pass filter, with a cutoff at 30 days. They indicate a flow that crosses the ice front into the cavity all year round but with an along-ice front component that is maximum during the winter months. Figure 8 shows that it is at the end of summer and within the period of southward flow that ISW is observed at FR6. At the western end of the ice shelf, therefore, ISW flow into the subice shelf cavity is at its maximum during the summer.

[29] The temperature and conductivity records from the sensors on FR6(261 m) (Figure 3) were corrected using the CTD profile taken in the same location at the time of the deployment of the FR6 mooring. Figure 11d shows the data plotted on a θ-*S* diagram after low-pass filtering with a cutoff of 12 hours. The rather dense line of data points at ~34.68, −1.91°C is an artifact of the low resolution of the temperature and conductivity sensors and should be ignored. The Gade line shows that at ~34.7 the salinity of the source water for the ISW observed at this instrument is the least saline of the HSSW observed at FR6.

[30] One of the aims of the study was to trace the flow of ISW from Ronne Ice Front to the north. The data gathered from the ROPEX98 cruise show that ISW is identifiable from the θ-*S* data only within a few km of the ice front. It is certainly not visible toward the northern end of the depression. The sequence of short sections parallel to the ice front (FF′, GG′, and HH′ in Figure 2) from PS99, shown in Figure 14, suggests that any ISW moving north is either rapidly dispersed or that the ISW flows in a narrow current confined to the ice front presumably to the northwest, as indicated by the current meters (Figure 9).

[31] During the winter months, ISW either never leaves the ice shelf cavity, possibly being blocked by the presence of a front at the southern edge of the zone of HSSW production, or else it does leave the cavity and is immediately reworked in the vigorous convection that takes place during the freezing season. Two strands of evidence support the former theory. The first is simply that the location of the FR5 mooring was within a few km of the point of emergence of the ISW, and there is no mechanism by which the ISW can be converted to HSSW in the time it takes to travel from the ice front to the site of the mooring, especially in summer.

[32] Additional evidence comes from oxygen isotope ratios. A selection of water samples obtained from the Ronne Depression during ROPEX98 were analyzed at the Stable Isotopes Laboratory, University of East Anglia, UK. Multiple analyses were undertaken for each water sample, and the results were found to be repeatable, on average, to ±0.03 per mille. The $\delta^{18}O$ data for samples of HSSW (Figure 15) obtained in the Ronne Depression during ROPEX98 show that although the ratio is depressed, the amount of depression is consistent with the fractionation that results from the process of freezing to form sea ice; the admixture of glacial melt is not necessary to account for the

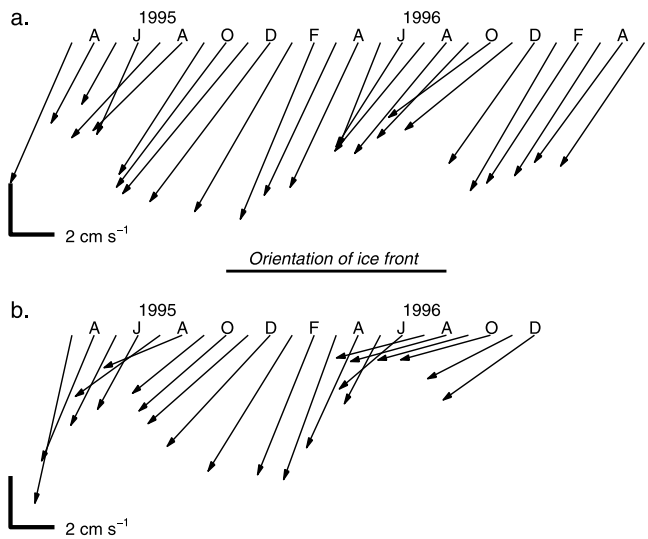

Figure 13. Stick plots illustrating the speed and direction of the currents measured at (a) the shallowest (FR6(261 m)) and (b) the deepest (FR6(588 m)) instruments at mooring FR6. The data have been low-pass filtered, with a cutoff of 30 days.

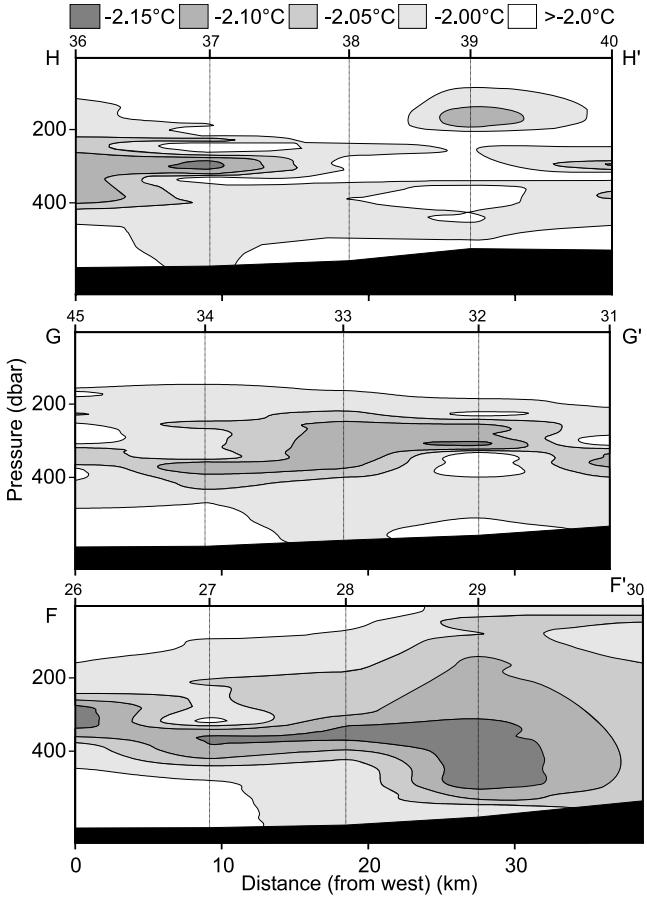

Figure 14. Sequence of ice front sections obtained in early 1999 (PS99). The sections highlight the distribution of ISW in the vicinity of the ice front. The locations of the sections are shown in Figure 2.

$\delta^{18}O$ values that are observed. Furthermore, the $\delta^{18}O$ measured in the HSSW shows no trend with increasing distance from the ice front. If ISW were being reworked into HSSW, we would expect an increasing $\delta^{18}O$ value (i.e., decreasing meltwater concentration) with increasing distance from the ice front. Our findings contrast with those of *Weiss et al.* [1979], who studied $\delta^{18}O$ values from samples taken in the Filchner Depression. They found that the values for HSSW present north of Filchner Ice Shelf could be explained only by the addition of glacial melt.

[33] In summary, the picture that emerges from these results is as follows. Ronne Depression ISW appears at the ice front at the depression's eastern flank. During the freezing season the ISW is unable to exit the cavity because of a front between the HSSW and the relatively fresh ISW. The dynamics associated with the front cause ISW to be directed along the ice front toward the northwest. During the summer, HSSW production is interrupted and ISW can emerge from the cavity. This is the period during which observations are generally obtained from ships. All along the ice front, ISW forms at about the depth of the ice shelf base as a result of water oscillating beneath the ice front under tidal action. This locally produced ISW is gathered by the predominantly along-ice front current before being sampled by the instruments at FR6. When the ISW arrives at the Antarctic Peninsula coast, it is directed to the south back into the subice cavity by the presence of the highly saline HSSW water mass in the Ronne Depression to the north. During the winter the flow into the cavity at the western end of the ice front, as detected at FR6, is composed entirely of HSSW, though there is a tendency for the flow at FR6 to be directed along, rather than under, the ice front during the height of the freezing season (Figure 13).

[34] At FR5 the ISW signature is strongest at the end of summer (Figure 8), consistent with the notion that the ISW retreats beneath the ice shelf during the winter period of full depth convection and HSSW production. Sporadic ISW signals are, however, also visible during the winter. This observation can be explained by the ISW's proximity to the ice front (and FR5) coupled with the presence of energetic short-period cross-front currents that result from tidal activity and from the 1- to 4-day eddy-like signals seen in the current data.

4. Heat Flux Beneath the Ice Shelf

[35] With only two moorings across the Ronne Depression and with no knowledge of the year-round hydrography along the ice front, it is not possible to give incontrovertible estimates of mass and heat fluxes into the subice shelf cavity. We cannot say whether there are strong wintertime inflows into the cavity in the central part of the depression, for example. However, these are the only available data. By simply assuming the western 50 km of the depression to be represented by FR6 and the eastern 100 km to be represented by FR5, we arrive at a volume flux into the cavity via

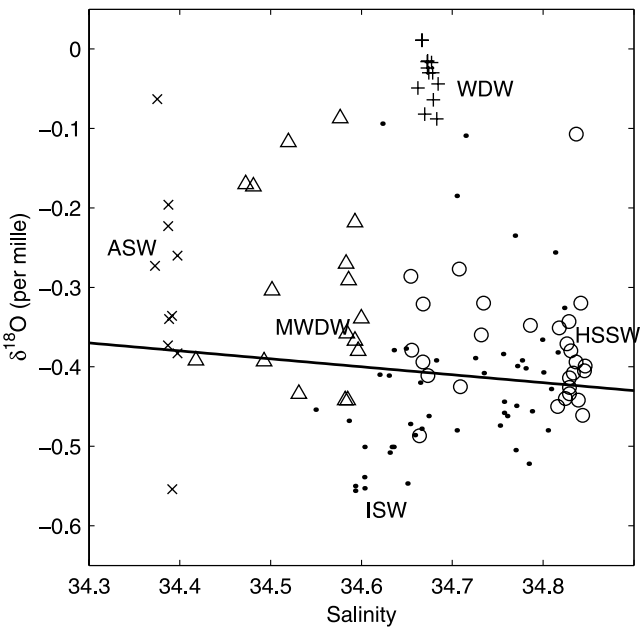

Figure 15. Plot of $\delta^{18}O$ against S for samples obtained in the Ronne Depression during ROPEX98. Pluses indicate WDW sampled at the continental shelf break; triangles indicate MWDW; crosses show Antarctic Surface Water (ASW); dots show ISW; and circles show HSSW. The line shows the evolution of a water mass's $\delta^{18}O$-S signature that would result from fractionation due to sea ice production.

the Ronne Depression of 0.9 ± 0.3 Sv. The error figure corresponds to moving the boundary dividing the regions represented by FR5 and FR6 by 20 km in either direction. A further assumption we make in arriving at the figure of 0.9 Sv is that the HSSW at the bottom of mooring FR5 is guided beneath the ice shelf by the seafloor topography (as discussed in section 2.3). By incorporating the ~0.5-Sv flow calculated by *Foldvik et al.* [2001] for the inflow along the portion of ice front between the Ronne Depression and Berkner Island, we arrive at a total inflow into the cavity of ~1.4 Sv.

[36] We can also estimate the net inflow of heat into the cavity via the Ronne Depression by combining the velocity and temperature data from the moored instruments. As there is a substantial net flow (0.9 Sv) into the cavity via the instrumented section, we must select an appropriate temperature for the remote, outflowing ISW. *Foldvik et al.* [2001] and *Nicholls et al.* [2001] have deduced that the cavity beneath the ice shelf is ventilated by two water masses. One is relatively saline HSSW flowing in via the Ronne Depression; the other is a fresher version of HSSW that flows from the Berkner Bank (Figure 1), entering the cavity between the Ronne Depression and Berkner Island. These authors show that the saline inflow from the Ronne Depression is too dense to escape the Filchner Depression, although it can be observed north of Filchner Ice Front as it recirculates beneath Filchner Ice Shelf. The less saline HSSW is converted to ISW, fresh enough to surmount the sill at the northern extreme of the Filchner Depression before descending the continental slope to the deep Weddell Sea. We suggest that the 0.9-Sv flow of HSSW entering via the Ronne Depression can only escape the system by being converted (ultimately) into the lighter form of ISW. It is the temperature of that ISW, therefore, that should be used in the calculation of the net heat flow into the ice shelf cavity. However, temperature measurements made in the Filchner Depression might be affected by mixing between the ISW and HSSW generated locally or by other water masses flowing into the depression. Using these temperatures in the calculation of the heat budget would, therefore, lead to an underestimate. The highest temperature that should be used is the highest temperature at which the ISW can interact with the ice shelf, i.e., the in situ freezing point at the ice shelf base at Filchner Ice Front (approximately −2.23°C for an approximate draft of 440 m).

[37] Assuming that the appropriate outflow temperature is indeed −2.23°C and associating the moored instruments with the same boxes as used for the volume flux calculation, we estimate a total heat flux into the cavity from the Ronne Depression of ~1.0 TW. If the outflow temperature was selected to be 0.1°C higher, the heat flux would reduce to 0.7 TW. One TW is capable of warming to the freezing point and then melting 2.8×10^6 kg s^{-1} of ice, assuming an average ice shelf core temperature of −24°C [*Jenkins and Doake*, 1991]. Using the same approach for interpreting the 0.5-Sv inflow estimated by *Foldvik et al.* [2001] for the section of Ronne Ice Front west of the Ronne Depression, we calculate an additional ice melt rate of 2.0×10^6 kg s^{-1}. The area of Filchner-Ronne Ice Shelf is $\sim 4.7 \times 10^{11}$ m^2. The average basal melt rate resulting from inflow along the entire length of Ronne Ice Front is therefore 0.34 m yr^{-1}. This figure is likely to be conservative as *Foldvik et al.* [2001] regard the value of 0.5 Sv to be on the low side. In addition, this estimate ignores inflow of shelf waters beneath Filchner Ice Front.

[38] Past average melt rates have been estimated on the basis of either glaciological or oceanographic data. From basal melt rates deduced from ice flow measurements, *Jenkins and Doake* [1991] estimated an average melt rate of 0.55 m yr^{-1} for the flow line they studied, though their value might have been inflated by the high melt rates at the rather deep grounding line in their study area. From subice shelf oceanographic measurements, *Nicholls et al.* [1997] estimate a basal melt rate for the western side of Ronne Ice Shelf of 0.2 m yr^{-1}. Their estimate excluded the band of relatively rapidly melting ice shelf near the ice front [*Jenkins and Doake*, 1991]. The estimate presented in this paper has attempted to account for the inflow along the entire length of Ronne Ice Front, if only represented by three mooring locations, and has therefore had a better prospect of catching the total heat flux into the cavity.

[39] Attempting to estimate flows across an ice front using data from instruments moored on the upstream side is fraught with problems. For much of its length, it is likely that flow will run parallel to the ice front, and so selecting the appropriate locations for moorings, and determining the portion of the cross section beneath the ice front represented by individual instruments, is difficult. As a result, the estimates of heat and volume fluxes given above should be regarded with caution. Bearing in mind the likely errors, a realistic estimate of the range in our value for the volume flux would be 1–2 Sv and for the average melt rate, 0.24–0.44 m yr^{-1}.

5. Summary and Conclusions

[40] We have used data from several recent cruises to the southwestern Weddell Sea, including along Ronne Ice Front, to improve our knowledge of the bathymetry of this underexplored region and to update our understanding of the conversion of water masses over the southern continental shelf and under Ronne Ice Shelf. Our principal observations are as follows. First, bathymetry data demonstrate for the first time that the Ronne Depression does not extend from the ice front to the continental shelf break; thus the circulation of ISW and other water types in the Ronne Depression is not directly analogous to circulation in the Filchner Depression. We have shown that the General Belgrano Bank, which in previous charts is shown as a major shoaling bank near the shelf break, is actually only a minor rise, with an elevation ~20 m above the surrounding flat shelf. Second, both the hydrographic and $\delta^{18}O$ measurements show no signs of a flow of ISW from Ronne Ice Front to the shelf break. Indeed, the hydrographic data that we present show the entire western continental shelf to be dominated by HSSW, even at the end of the summer. A substantial intrusion of MWDW was found east of the pool of HSSW. During cruises in 1995 and 1999, MWDW was found penetrating onto the continental shelf as far east as Berkner Bank.

[41] The CTD and current meter data from near Ronne Ice Front in the Ronne Depression show that the most saline HSSW does not pass into the ice shelf cavity and that the principal inflow of HSSW appears to be at the western end

of the ice front. Maximum inflow of HSSW occurs during late summer. The total flux of water into the subice cavity via the Ronne Depression is estimated at 0.9 ± 0.3 Sv. The associated net influx of heat available for warming and then melting the ice shelf is estimated to be 1.0 ± 0.4 TW. When combined with the inflow calculated by *Foldvik et al* [2001] for Ronne Ice Front west of the Ronne Depression, we find a total net melt rate of $\sim 5 \times 10^6$ kg s^{-1} and an average basal melt rate of 0.34 ± 0.1 m yr^{-1}.

[42] **Acknowledgments.** The authors wish to express their gratitude to the personnel of HMS *Endurance* and *Polarstern* for their support during the three cruises and are thankful for the helpful suggestions from two anonymous reviewers.

References

Ackley, S. F., C. Geiger, J. C. King, E. C. Hunke, and J. C. Comiso, The Ronne Polynya of 1997–98: Observations of air-ice-ocean interaction, *Ann. Glaciol.*, *33*, 425–429, 2001.

Baines, P. G., and S. Condie, Observations and modelling of Antarctic downslope flows: A review, in *Ocean, Ice, and Atmosphere: Interactions at the Antarctic Continental Margin*, *Antarct. Res. Ser.*, vol. 75, edited by S. S. Jacobs and R. F. Weiss, pp. 29–49, AGU, Washington, D. C., 1998.

British Antarctic Survey, Antarctic Peninsula and Weddell Sea, *Map BAS Misc. Ser. 8*, scale 1:3,000,000, Cambridge, UK, 2000.

Chapman, D. C., Dense water formation beneath a time-dependent coastal polynya, *J. Phys. Oceanogr.*, *29*, 807–820, 1999.

Foldvik, A., and T. Gammelsrød, Notes on Southern-Ocean hydrography, sea-ice and bottom water formation, *Palaeogeogr. Palaeoclimatol. Palaeoecol.*, *67*, 3–17, 1988.

Foldvik, A., T. Gammelsrød, and T. Tørresen, Circulation and water masses on the southern Weddell Sea Shelf, in *Oceanology of the Antarctic Continental Shelf*, *Antarct. Res. Ser.*, vol. 43, edited by S. S. Jacobs, pp. 5–20, AGU, Washington, D. C., 1985a.

Foldvik, A., T. Gammelsrød, and T. Tørresen, Physical oceanography studies in the Weddell Sea during the Norwegian Antarctic Research Expedition 1978/79, *AAAS Sel. Symp.*, *3*, 195–207, 1985b.

Foldvik, A., T. Gammelsrød, E. Nygaard, and S. Østerhus, Current measurements near Ronne Ice Shelf: Implications for circulation and melting, *J. Geophys. Res.*, *106*, 4463–4477, 2001.

Foster, T. D., and E. C. Carmack, Frontal zone mixing and Antarctic Bottom Water formation in the southern Weddell Sea, *Deep Sea Res. Oceanogr. Abstr.*, *23*, 301–317, 1976.

Gade, H. G., Melting of ice in sea water: A primitive model with application to the Antarctic ice shelf and icebergs, *J. Phys. Oceanogr.*, *9*, 189–198, 1979.

Gammelsrød, T., A. Foldvik, O. A. Nøst, Ø. Skagseth, L. G. Anderson, E. Fogelqvist, K. Olsson, T. Tanhua, E. P. Jones, and S. Østerhus, Distribution of water masses on the continental shelf in the southern Weddell Sea, in *The Polar Oceans and Their Role in Shaping the Global Environment*, *Geophys. Monogr. Ser.*, vol. 85, edited by O. M. Johannessen et al., pp. 159–176, AGU, Washington, D. C., 1994.

Gordon, A. L., Western Weddell Sea thermohaline stratification, in *Ocean, Ice and Atmosphere: Interactions at the Antarctic Continental Margin*, *Antarct. Res. Ser.*, vol. 75, edited by S. S. Jacobs and R. F. Weiss, pp. 215–240, AGU, Washington, D. C., 1998.

Gordon, A. L., B. A. Huber, H. H. Hellmer, and A. Field, Deep and bottom water of the Weddell Sea's western rim, *Science*, *262*, 95–97, 1993.

Grosfeld, K., M. Schröder, E. Fahrbach, R. Gerdes, and A. Mackensen, How iceberg calving and grounding change the circulation and hydrography in the Filchner Ice Shelf-Ocean System, *J. Geophys. Res.*, *106*, 9039–9055, 2001.

Harms, S., E. Fahrbach, and V. H. Strass, Sea ice transports in the Weddell Sea, *J. Geophys. Res.*, *106*, 9057–9073, 2001.

Hunke, E. C., and S. F. Ackley, A numerical investigation of the 1997–1998 Ronne Polynya, *J. Geophys. Res.*, *106*, 22,373–22,382, 2001.

Jenkins, A., and C. S. M. Doake, Ice-ocean interaction on Ronne Ice Shelf, Antarctica, *J. Geophys. Res.*, *96*, 791–813, 1991.

Lewis, E. E., The Practical Salinity Scale 1978 and its antecedents, *IEEE J. Oceanic Eng.*, *5*, 3–8, 1980.

Makinson, K., and K. W. Nicholls, Modeling tidal currents beneath Filchner-Ronne Ice Shelf and on the adjacent continental shelf: Their effect on mixing and transport, *J. Geophys. Res.*, *104*, 13,449–13,465, 1999.

Millero, F. J., Freezing point of sea water, Eighth report of the Joint Panel of Oceanographic Tables and Standards, Appendix 6, *UNESCO Tech. Pap. Mar. Sci.*, *28*, 29–31, 1978.

Muench, R. D., and A. L. Gordon, Circulation and transport of water along the western Weddell Sea margin, *J. Geophys. Res.*, *100*, 18,503–18,515, 1995.

Nicholls, K. W., and K. Makinson, Ocean circulation beneath the western Ronne Ice Shelf, as derived from in situ measurements of water currents and properties, in *Ocean, Ice, and Atmosphere: Interactions at the Antarctic Continental Margin*, *Antarct. Res. Ser.*, vol. 75, edited by S. S. Jacobs and R. F. Weiss, pp. 301–318, AGU, Washington, D. C., 1998.

Nicholls, K. W., K. Makinson, and M. R. Johnson, New oceanographic data from beneath Ronne Ice Shelf, Antarctica, *Geophys. Res. Lett.*, *24*, 167–170, 1997.

Nicholls, K. W., L. Padman, and A. Jenkins, First physical oceanography results from the ROPEX98 cruise to the southern Weddell Sea, in *Filchner Ronne Ice Shelf Programme*, vol. 12, edited by H. Oerter, pp. 51–58, Alfred-Wegener-Inst. for Polar and Mar. Res., Bremerhaven, Germany, 1998.

Nicholls, K., S. Østerhus, K. Makinson, and M. R. Johnson, Oceanographic conditions south of Berkner Island, beneath Filchner-Ronne Ice Shelf, Antarctica, *J. Geophys. Res.*, *106*, 11,481–11,492, 2001.

Padman, L., R. Robertson, and K. Nicholls, Modelling tides in the southern Weddell Sea: Updated model with new bathymetry from ROPEX, in *Filchner Ronne Ice Shelf Programme Report*, vol. 12, edited by H. Oerter, pp. 65–73, Alfred-Wegener-Inst. for Polar and Mar. Res., Bremerhaven, Germany, 1998.

Renfrew, I. A., J. C. King, and T. Markus, Coastal polynyas in the southern Weddell Sea: Variability of the surface energy budget, *J. Geophys. Res.*, *107*(C6), 3063, doi:10.1029/2000JC000720, 2002.

Vaughan, D. G., J. Sievers, C. S. M. Doake, G. Grikurov, H. Hinze, V. S. Pozdeev, H. Sandhäger, H. W. Schenke, A. Solheim, and F. Thyssen, Map of subglacial and seabed topography 1:2,000,000 Filchner-Ronne-Schelfeis, Antarktis, Inst. für Angew. Geod., Frankfurt am Main, Germany, 1994.

Weiss, R. F., H. G. Østlund, and H. Craig, Geochemical studies of the Weddell Sea, *Deep Sea Res.*, Part A, *26*, 1093–1120, 1979.

Woodgate, R. A., M. Schröder, and S. Østerhus, Moorings from the Filchner Trough and the Ronne Ice Shelf Front: Preliminary results, in *Filchner Ronne Ice Shelf Programme Report*, vol. 12, edited by H. Oerter, pp. 85–90, Alfred-Wegener-Inst. for Polar and Mar. Res., Bremerhaven, Germany, 1998.

A. Jenkins and K. W. Nicholls, British Antarctic Survey, High Cross, Madingley Road, Cambridge CB3 0ET, UK. (ajen@bas.ac.uk; kwni@bas.ac.uk)

S. Østerhus, Geophysical Institute, University of Bergen, Allegaten 70, N-5007 Bergen, Norway. (svein.osterhus@gfi.uib.no)

L. Padman, Earth and Space Research, 1910 Fairview Avenue East, Suite 102, Seattle, WA 98102-3620, USA. (padman@esr.org)

M. Schröder, Alfred-Wegener-Institut für Polar und Meeresforschung, Columbusstraße, Postfach 120161, D-27515 Bremerhaven, Germany. (mschroeder@awi-bremerhaven)

R. A. Woodgate, Polar Science Center, Applied Physics Laboratory, University of Washington, 1013 NE 40th Street, Seattle, WA 98105-6698, USA. (woodgate@apl.washington.edu)